Impact of Triplet State Population on GFP-type Fluorescence and Photobleaching

Martin Byrdin[1*] & Svetlana Byrdina[2]

Addresses

1 Institut de Biologie Structurale, CNRS, Université Grenoble Alpes, CEA, IBS, 38044 Grenoble, France

2 Univ. Grenoble Alpes, Univ. Savoie Mont Blanc, CNRS, IRD, Univ. Gustave Eiffel, ISTerre, 38000 Grenoble, France

Abstract

Based on recently published parameters (Rane et at. 2023, JPCB 127, 5046-5054) for (rs)EGFP triplet state formation and decay rates and yields, we consider the power density dependence of triplet state population dynamics and its consequences for the application of green fluorescent proteins in biological single molecule fluorescence microscopy.

We find that under certain conditions, the photon budget of GFP type fluorescent proteins can be linearly dependent on power density and we propose a possible explanation for such a non-Hirschfeld photobleaching behavior. Moreover, illumination with ms pulses at kHz rates is shown to improve photostability. We stipulate that a judicious choice of excitation wavelength should take into account the triplet state absorption spectrum along with the singlet state absorption spectrum.

Formulae are given for the estimation of the effects of such choice as function of the experimental parameters.

Keywords:

Biological microscopy, Cryotemperature, Fluorescent probes, Photon budget, Photophysics, Power density dependence, rsEGFP2 off state

Toc-graphic 5x5 cm +50 words

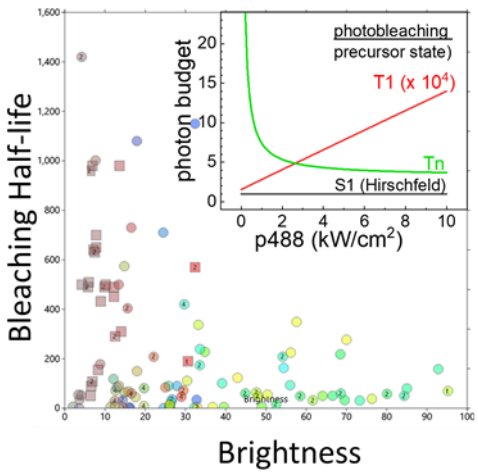

Hirschfeld predicted that photobleaching rates should scale with fluorescence brightness, which is obviously not the case for fluorescent proteins found in the fpbase.org. We investigate an alternative theory considering the triplet state as precursor for photobleaching.

Introduction

Almost fifty years ago, Tomas Hirschfeld derived a remarkable formula for fluorescent molecules.[1] He found that under quite general conditions, the observed photobleaching rate of a fluorescent molecule scales proportionally with both its absorption coefficient ε and its fluorescent quantum yield φ_{Fl} (and hence their product, the so-called molecular brightness MB).

$$k_{Bl} = a\ \varepsilon\ \varphi_{Fl} \qquad \text{Eq.(1)}$$

Apparently unperturbed, during many years, the fluorescent protein (FP) community pursued efforts to develop improved FPs that would show both greater brightness and greater photobleaching resistance at the same time. The first mention of the Hirschfeld work in the FP community occurred as late as 2013.[2,3] Such long ignorance could later luckily be justified by the facts: Indeed, taking from the fpbase [4] all the FPs with reported photobleaching rates and plotting them against their MB does not show any whatsoever meaningful correlation (Figure 1 actually shows the half-life on the y-axes, but plotting the actual photobleaching rate would not change a thing, neither does choosing subsets of suitable color, oligomerization state, etc…).

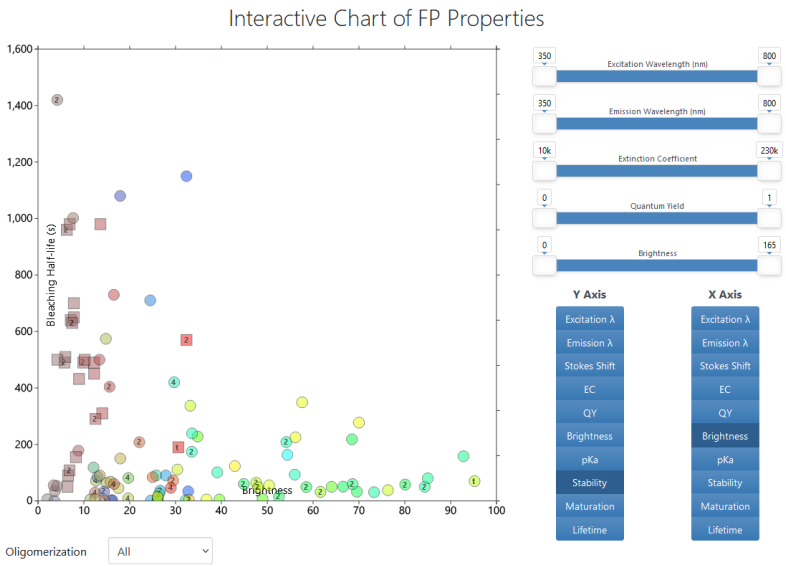

Figure 1. Screenshot at the time of writing (July 2023) of photobleaching half-life (y) vs molecular brightness (x) of all available FPs from the fpbase.org.

Apart from the notoriously poorly defined conditions for the determination of photobleaching lifetimes (but see ref [5] for the exception), we are left with the conclusion that for GFP-type FPs, some of the conditions leading to eq 1 must be prominently not fulfilled. Recent developments allow us to discuss the matter and to elaborate an adaptation of the Hirschfeld treatment to such FPs.

Actually, an implicit condition in the derivation of eq.(1) was that photobleaching starts from the same light induced state S1 as fluorescence and that all other possible "shelve" or "dark" states are just photophysically inert bystanders, i.e. neither absorbing, fluorescing or, for that matter, contributing to photobleaching reactions. The recent publication of the absorption spectrum of the EGFP triplet state showed that this condition is not fulfilled.[6,7] Indeed, a prominent triplet state absorption band covers the whole visible spectral window such that excitation light at practically any wavelength is bound to re-excite T1 to a higher excited Tn state from where it can react further (see Scheme 1 for designation of states and rate constants).

1. Triplet state buildup and reaction pathways

The important lifetime and formation yield of the triplet state T1 of FPs have for consequence that under the conditions typically found in biological single molecule fluorescence microscopy (immobilized samples under wide-field illumination in the order of kW/cm^2), significant T1 buildup occurs.

Depending on applied excitation energy density, few milliseconds are sufficient to pump the vast majority of the potentially fluorescing molecules into T1 from where they are not only no longer able to fluoresce ("first image artefact"),[8,9] but, due to the high reactivity of the T1 state, are also prone to oxidation and reduction reactions which, if not reversed rapidly, may lead to accelerated photobleaching. Increased T1 population thus appears as a double penalty: less fluorescence and more permanent losses. In this contribution, we discuss possibilities and strategies to optimize conditions for fluorescence microscopy to get out of GFP markers a maximum of signal with a minimum of degradation, both for room temperature (RT) and cryo temperature (100 K, CT), and for continuous and pulsed illumination.

As a starting point, let us consider the photophysical Scheme 1 of electronic states of a GFP-type FP.

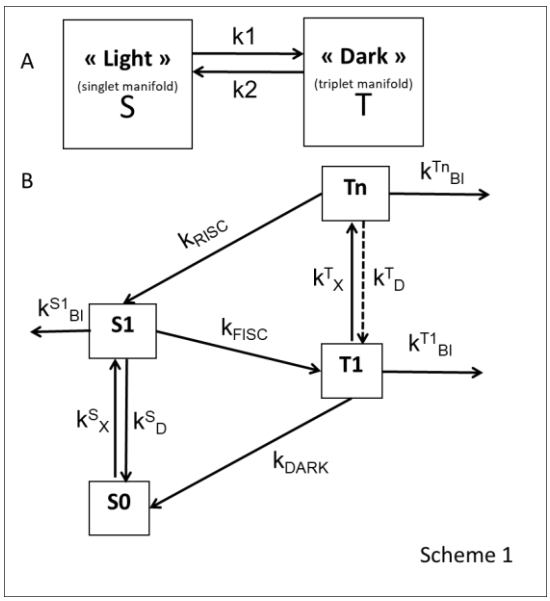

Scheme 1. Electronic states and rate constants involved in FP fluorescence and photobleaching. A, basic two state scheme, B, elaborate four state scheme. Excitation with rate constant k^S_X pumps molecules from the singlet ground state S0 to the fluorescing excited state S1, from where de-excitation (radiative and non-radiative) occurs with rate constant k^S_D. Alternatively, forward intersystem crossing (FISC) can populate with rate constant k_{FISC} the lower lying lowest triplet state T1, from where either dark relaxation with rate constant k_{DARK} repopulates S0 or re-excitation with rate constant k^T_X leads to a higher triplet state Tn, from where again de-excitation with rate constant k^T_D to T1 is possible or reverse intersystem crossing (RISC) with rate constant k_{RISC} to S1. In parallel to this S/T cycling, all excited states can undergo irreversible photochemistry with rate constants k^i_{Bl}.

The relative populations of the four relevant states S0, S1, T1, and Tn are given by the rate constants connecting them and these in turn are defined by the molecular parameters of the FP chromophore such as absorption cross sections σ_i, radiative lifetimes τ_i and quantum yields φ_i.

Under continuous illumination, an equilibrium distribution of the FP molecules over the four relevant states S0, S1, T1, and Tn will establish as follows: For a total chromophore population normalized to unity, the final populations for the singlet (S) and triplet (T) manifolds will be given by equation (2):

$$T = k_{FISC} / k_{\Sigma}, \qquad S = (k_{RISC} + k_{DARK}) / k_{\Sigma} \qquad \text{Eq. (2)}$$

This gives for the population ratio S/T shown in Figure 2:

$$S/T = (k_{RISC} + k_{DARK}) / k_{FISC} = k_{\Sigma} / k_{FISC} - 1 \qquad \text{Eq. (3)}$$

with $k_\Sigma = k_{FISC} + k_{RISC} + k_{DARK}$ and $k_{FISC} = p488\ \sigma_S\ \varphi_F$, $k_{RISC} = p488\ \sigma_T\ \varphi_R$, Eq. (4)

where φ_F and φ_R are the quantum yields for forward and reverse inter system crossing, σ_S and σ_T are the absorption cross sections of the singlet S0 and triplet T1 states, respectively.

Within each of these manifolds, neglecting intersystem crossing, the fractional population of the excited states is given by the balance of population and depopulation rate constants:

$S1/S0 = k^S_X / (k^S_X + k^S_D)$, $Tn/T1 = k^T_X / (k^T_X + k^T_D)$ Eq.(5)

The de-excitation rate of the singlet state $k^S_D = 1/\tau_{Fl} = k_{fl} + k_{nr}$ is dominated by fluorescence, that of the triplet state by internal relaxation: $k^T_D = k_{IR}$, whereas the dark relaxation rate contains contributions from phosphorescence and quenching: $k_{DARK} = 1/\tau_{Ph} = k_{Ph} + k_q$. The excitation rate constants are given by the product of the applied power density (more specifically: the wavelength dependent photon flux density in hc/λ units) p488 and the cross section of the absorbing states σ:

$k^S_X = p488\ \sigma_S$, $k^T_X = p488\ \sigma_T$ Eq.(6)

Thus, the behavior of the system is fully defined by the chromophore's photophysical characteristics and the experimental conditions, mainly excitation light intensity and wavelength, but also temperature, viscosity, quencher concentration, etc. Throughout this paper, and where not mentioned otherwise, we will consider conditions typically found in biological fluorescence microscopy, namely monochromatic excitation at 488 nm with 1 kW/cm ^{2} into the absorption band of the deprotonated EGFP chromophore with ε_S = 50 mM $^{-1}$ cm^{-1}. For such excitation, $k^S_X \approx 0.8\ MHz$ which means that for a microscope with a few percent detection efficiency, a per-molecule count rate of few kHz could be expected in the absence of intersystem crossing.

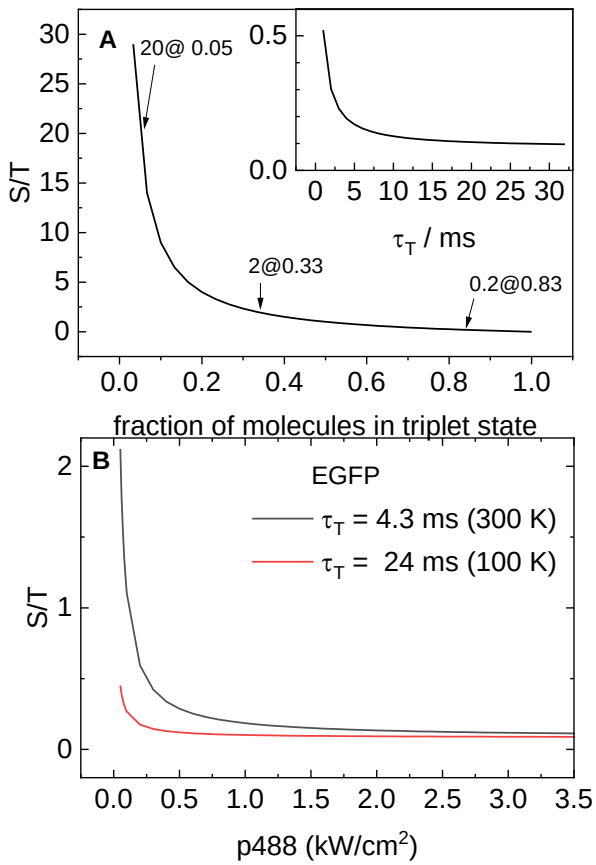

Figure 2. The equilibrium singlet-to-triplet ratio (eq. 3) decreases rapidly with increased triplet fraction (A, main), increased triplet state lifetime (A inset, for p488 = 1 kW/cm ^{2} and ε_S = 50 mM $^{-1}$ cm^{-1}) and increased pump power density p488 (B).

Figure 2 shows that with linearly increasing T1 fraction, the photo-physically relevant S/T ratio diminishes hyperbolically, i.e. much faster than linearly.

From equations (4) and (6), it can be seen that all four of the rate constants k^S_X, k^T_X, k_{FISC}, and k_{RISC} are power density dependent. From equations (2) and (5), it follows that so are the relative populations of all four relevant states S0, S1, T1, and Tn. Figure 3 shows the dependence on power density of these populations (note the common x-scale but different y-scales for lower and higher state populations). Note that for cw power densities going from 10 W/cm^2 to 10 kW/cm^2, the equilibrium triplet population increases from 9 to 91%. This is the power density window considered in this paper and illustrated in most of the following figures.

Figure 3. Dependence of equilibrium populations of lowest (A, eq.2) and of higher (B, eq. 5) singlet (black) and triplet (red) states on the applied excitation power density. B, total excited state populations, i.e. ground state populations from panel A multiplied by excited state fractions according to eq. (5). Note that in panel B the y-scale is 1000 times smaller. The Tn curve is calculated with $k_{IR} = 10^{10}$ Hz and $k_{DARK} = 233$ Hz, i.e. for RT.

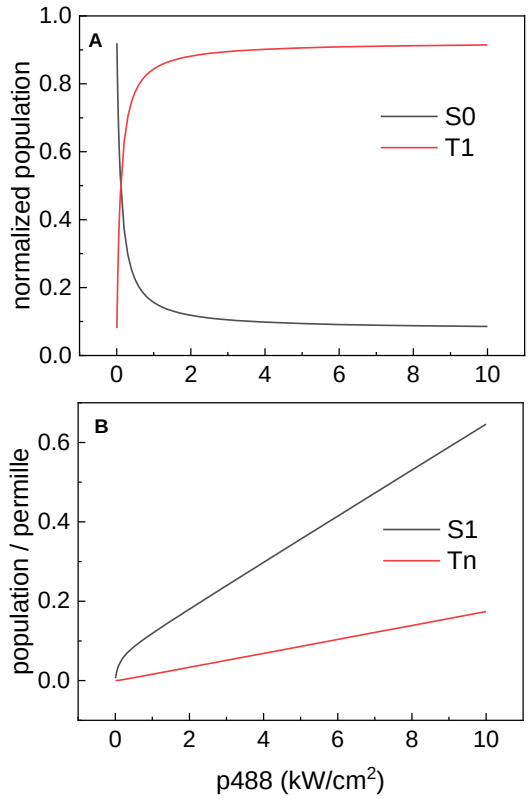

From Figure 3B and equation (5), it can be seen that for any excitation energies < 100 kW/cm^2, the excited state fractions are less than 1%, so that in the following, we will freely use S for S0 and T for T1.

From equations (2) - (6) it also follows that *Tn* depends on *p488* both via $k_{FISC/RISC}$ and *via* k^T_X Thus, in general, an inverse quadratic dependence on power density could be expected.

$$Tn = k^T_X / (k^T_X + k^T_D) \cdot k_{FISC} / k_\Sigma \qquad \text{eq. (7)}$$

$$= p488\ \sigma_T / (p488\ \sigma_T + k_{IR}) \cdot p488\ \sigma_S\ \varphi_F\ / (p488\ \sigma_T\ \varphi_R + p488\ \sigma_S\ \varphi_F + k_{DARK})$$

However, from Figure 3B it appears that the power density dependence is rather linear. This is due to the fact that p488 always appears concomitantly both in the numerator and in the

denominator and in both denominators it is moreover modulated by an additional term that is independent on power density.

2. Importance of reverse inter-system crossing

With the rate constants for triplet state formation and decay as reported by Rane et al, a major fraction of all potentially fluorescent molecules will be shelved away from the fluorescent manifold within few milliseconds, depending on the applied excitation power density.[7] This shelving process is, however, counteracted upon by the inverse process of light induced back-pumping (RISC), albeit with reduced brightness (quantum yield x cross section, ca 10% of FISC). It is hence the RISC process that determines the distribution of the available FP molecules into steady state populations of S and T (see eq. 2). Figure 4 shows typical kinetics of equilibrium establishment with and without taking into account the RISC pathway. For this graph, a low power density of 0.3 kW/cm^2 was chosen such that the timescale corresponds to the establishment of the S⇔T equilibrium. At higher power densities, the differences of equilibrium fluorescence between with and without RISC will be more important. At 1 kW/cm^2, e.g., the final fluorescence levels will differ by a factor of almost 2 for room temperature (RT) and more than 4 for cryo temperature (CT).

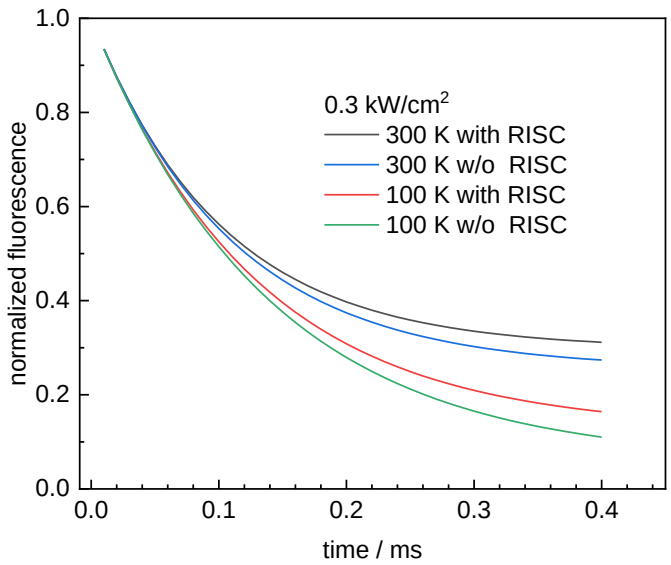

Figure 4. Continuous illumination (here 0.3 kW/cm^2 into a 50 mM $^{-1}$ cm^{-1} absorption band) rapidly pumps most excited fluorophores into the non-fluorescent triplet state. Light-induced reverse intersystem crossing counteracts and partially compensates the loss of fluorescence (black vs blue at RT, red vs green at CT).

The incorporation of this additional light induced depopulation of the triplet state complicates the two-state model of scheme 1A (k2 is no longer a purely dark reaction) and necessitates some further elaboration. We will address consequences for fluorescence and photobleaching in the following two sections, separately first for continuous wave (cw-) illumination (section 3) and then in section 4 for illumination by millisecond pulses with kHz repetition rates. The obtained results will be illustrated on the example of the popular reversibly switchable FP rsEGFP2 in section 5 and a general discussion follows in section 6.

3. Continuous excitation

Let us consider a parameter G (for "goodness") that describes the two essential properties of a FP: on the up side: the fluorescence FL that can be harnessed from it, and on the down side the photobleaching BL that restricts its practical applicability.

G=FL/BL eq (8)

The obtainable total Fluorescence FL is given by its quantum yield φ_{Fl} and by the population of its precursor state S1:

$FL = \varphi_{Fl}\,[S1]$

In an analogous manner, the photobleaching BL is given by its quantum yield φ_{Bl} and the population of its precursor state, which in the Hirschfeld framework is also S1:

$BL = \varphi_{Bl}\,[S1]$

From where immediately follows

$G^S = \varphi_{Fl}\,[S1] / \varphi_{Bl}\,[S1] = \varphi_{Fl} / \varphi_{Bl}$. eq (9)

Using the definitions $\varphi_{Fl} = k_{Fl} /(k_{Fl} + k_{Bl} + k_{nr})$ and $\varphi_{Bl} = k_{Bl} /(k_{Fl} + k_{Bl} + k_{nr})$, k_{nr} being the FP's nonradiative decay rate, eq (9) transforms into

$G^S = k_{Fl} / k_{Bl}$. eq (10)

which expression is very close to what Hirschfeld defined as the photon budget (PB) of a fluorophore, i.e. the total amount of photons that can be obtained from it before photobleaching is completed.

$PB = n_0\,(k_{Fl} + k_{Bl} + k_{nr}) / k_{Bl}$, (i.e. the inverse of the bleaching yield φ_{Bl} defined above).

Here the normalization factor n_0 describes the number of initially excitable chromophores, in our treatment, we will consider normalized populations, setting $n_0 = 1$.

For cases where, as in FPs, k_{Fl} is bigger than k_{Bl} and k_{nr} , it dominates the numerator, and we have G^S approximately equal to PB. This photon budget, and that was the other remarkable finding by Hirschfeld, depends only on the intrinsic rates for fluorescence and photobleaching, but it is totally independent on most other molecular and experimental conditions, such as chromophore absorption coefficient, fluorescence quantum yield, and, most importantly, even applied power density (eq. 10).
Now we saw in the introduction (the observed *independence* of photobleaching halflife on the chromophore's brightness), that Hirschfeld's initial assumption of photobleaching starting exclusively from S1 is not generally warranted for FPs. (For simplicity, in this contribution we restrict ourselves to GFP-type green fluorescent proteins for which the photophysical parameters are known.)

We therefore will now consider two limiting cases:

i) the BL precursor state is exclusively T1, or
ii) the BL precursor state is exclusively Tn.

In the two cases, in contrast to what was predicted by Hirschfeld for S1 being the only photobleaching precursor state, we expect a dependence on power density via the T population (see Figure 3). Comparing the theoretical dependences on power density predicted here with those observed experimentally, eg by Cranfill et al. [5], we can strive to make conclusions on the relative contributions of the respective proposed pathways i) and ii).

i) The photobleaching precursor state is exclusively T1

With eq (8) and the steady state populations from eq (2) we have

$$G^{T1} = \varphi_{Fl}\,[S1]/\,\varphi_{Bl}\,[T1] = G^S \cdot\; k^S_X\,/(k^S_X+k_{Fl}) \cdot\; (k_{DARK} + k_{RISC})\,/\,k_{FISC} \qquad \text{eq (11)}$$

In this equation, the second factor defines the excited fraction of the singlet manifold (eq. 5), and the last factor gives the ratio of the normalized steady state populations of the singlet and triplet manifolds under continuous excitation (eq. 3).

To gain insight into the dependence of G^{T1} on the excitation power density p488 and on the respective singlet and triplet state absorption cross sections σ_S and σ_T, we use eq (4) and (6) to explicitly express the rate constants k^S_X and k_{FISC} and k_{RISC} through them. Then we have from eq (11)

$$G^{T1} = G^S \cdot\; p488\,\sigma_S\,/(p488\,\sigma_S + k_{Fl})\,(\sigma_T\,\varphi_R/\,\sigma_S\,\varphi_F + k_{DARK}\,/\,p488\,\sigma_S\,\varphi_F\,)$$

$$= G^S\,(k_{RISC} + k_{DARK})\,/\,(k_{FISC} + k_{Fl}\,\varphi_F)\,,$$

$$= G^S\;(\,p488\,\sigma_T\,\varphi_R + k_{DARK}\,)\,/\,(\,p488\,\sigma_S + k_{Fl}\,\varphi_F\,) \qquad \text{eq (12)}$$

In equation (12), nominally, both k_{RISC} and k_{FISC} are dependent on p488 via the absorption cross sections of their respective precursor states σ_S and σ_T. However, in Fig. 5 we observe rather a linear increase of G^{T1}. The at first glance counterintuitive observation that the goodness G^{T1} increases with increasing excitation power density is explained by the fact that the RISC pathway effectively limits accumulation of the vulnerable triplet state (to the saturation level of $1- k_{RISC}/k_{FISC} = 91\%$) whereas fluorescence continues to increase via enhanced singlet state excitation.

ii) the photobleaching precursor state is exclusively Tn

With eq (8) we have

$$G^{Tn} = \varphi_{Fl}\,[S1]\,/\,\varphi_{Bl}\,[Tn]$$

$$= G^S \cdot\; k^S_X\,/\,(k^S_X+k_{Fl}) \cdot\; (k^T_X+k_{IR})\,/\,k^T_X\;\cdot\;(k_{DARK} + k_{RISC}\,)/\,k_{FISC} \qquad \text{eq (13)}$$

In contrast to eq (11), here we have introduced the additional term $k^T_X\,/\,(k^T_X+k_{IR})$ for triplet state re-excitation, whereas the overall population factors stay the same as in the previous case (i.e. we assume that the photobleaching via Tn occurs independently from the RISC pathway). Following a completely analogous treatment to that in the previous case, we obtain the following expression for the goodness:

$$G^{Tn} = G^S \cdot (p488\,\sigma_T + k_{IR})\,/\,(p488\,\sigma_S + k_{Fl}) \cdot (\,\varphi_R\,/\,\varphi_F + k_{DARK}\,/\,p488\,\sigma_T\,\varphi_F)$$

$$= G^S \cdot\; (p488\,\sigma_T + k_{IR})\,/\,(p488\,\sigma_S + k_{Fl}) \cdot\; \varphi_R\,/\,\varphi_F \cdot (\,1 +\; k_{DARK}\,/\,k_{RISC}) \qquad \text{eq (14)}$$

As with eq (7) for [Tn], the excitation power density enters G^{Tn} twice, both via singlet and triplet state absorption, i.e. under certain circumstances, an inverse quadratic power density dependence can be expected. However, in both instances a second term adds to the power density term and modulates its impact. Again, for not too high excitation, in the first factor, the intrinsic decay rates k_{Fl} and also k_{IR} will outcompete the power density dependent contributions by far because higher triplet states are reputed to be extremely shortlived (in analogy to the Kasha rule for the singlet manifold). As a result, the first factor is roughly ten (i.e. k_{IR} / k_{Fl}), and we are left not with an inverse quadratic but rather with an inverse *linear* power density dependence (via k_{RISC} in the last denominator) in this case. The power density dependences for both triplet states proposed as photobleaching precursors are shown in Figure 5.

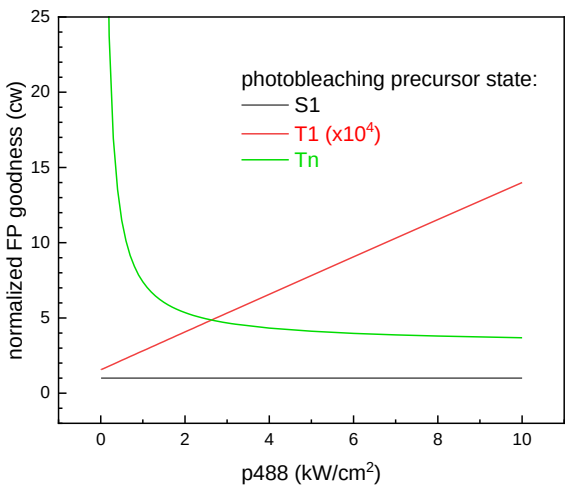

Figure 5. Dependence of Goodness on cw excitation power density for the cases that the precursor state of photobleaching is either S1, T1, or Tn. Note that the values for a T1 precursor are sub-permille and for comparison had to be upscaled by a factor of 10000.

In conclusion to this section, we relate the theoretically predicted power density dependences of photobleaching (equations (12) and (14), Fig. 5) to those observed experimentally in the most comprehensive study in ref [5]. There, the authors expected to find a linear power density dependence of the *observed* bleaching rate, i.e. a power density independent goodness. Instead, they found that most FPs showed "supralinear photobleaching" with power exponents scattered between 0.65 and 1.92 with a median around 1.1 (their mean ± s.d. is 1.16 ± 0.24). Whereas most of the observed photobleaching was stronger than linearly power density dependent, some proteins showed sublinear photobleaching. This intriguing behavior might find an explanation if the observed bleaching rates would actually result from a (partial) compensation of two opposing effects, viz inverse linear photobleaching from Tn (case ii, green curve in Fig. 5) and direct linear increase of the photon budget from T1 population as predicted for case i (red curve in Fig. 5). In such a scenario, power coefficients scattered around 1.x would not be totally unexpected. To verify these speculations, more experimental work is definitely needed.

4. Pulsed excitation

It was proposed early on that potentially harmful exposure of T1 to excitation light could be minimized via a pulsed illumination scheme, e.g. for D-rex or FCS applications. [10,11] Those early attempts traditionally concentrated on MHz pulsing, partly because organic dye triplet lifetimes are found rather in the microsecond range. On the other hand, such timing is natural for MW / cm^2 excitation energy densities where the singlet population decays within sub-microseconds (downscale the x-axes of Fig. 4 by a factor of thousand). Here, we consider

rather kW / cm^2 excitation energy densities and consequently, kHz pulsing schemes with ms exposure times.

To limit accumulation of the triplet state, light exposure time periods should be short with respect to establishment of equilibrium (i.e. submilliseconds) and interleaved with periods allowing for recovery of the singlet population, ie few ms at RT and few tens of ms at CT. Under such conditions, no significant triplet state accumulation should occur, but concomitantly the time-averaged fluorescence is reduced due to the dark periods without excitation. In a remarkable 2005 paper, Gregor et al. proposed a formalism to find time-averaged populations for such illumination schemes (Scheme 2) and derived formulae for their calculation. [12]

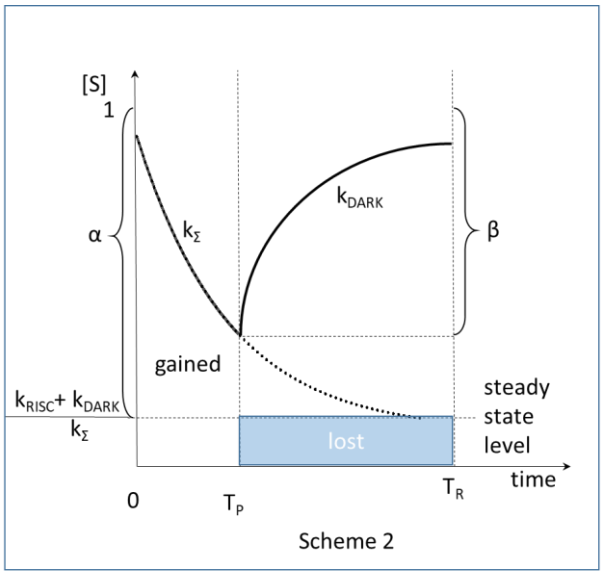

Scheme 2. Population evolution under pulsed illumination. The area under the thick black curve is singlet population (i.e. potentially fluorescing), the area above the thick black curve is triplet population (i.e. potentially photobleaching). Under pulsed illumination, singlet state population cycles between a maximal value at the end of a repetition period of duration T_R and a minimal value 1-β at the end of a pulse of duration T_P. As compared to continuous illumination, where at steady state the fluorescence stays at the blue level, during pulses short with respect to 1/ k_Σ, considerable fluorescence can be gained.

Here, we apply their formalism for the system in Scheme 1B, taking into account the additional RISC pathway (that was not considered then). Using the obtained expressions, we can generalize the cw treatment of the previous section for the case of interleaved excitation and find optimal parameters for pulse duration T_P and repetition period T_R.
For the calculation of G_{pulsed}, we need to obtain expressions for S1 averaged over the time period from zero to T_P (the light period only) for the numerator, and for the denominator we need T1 averaged over the complete pulse cycle (light and dark, from zero to T_R) for G^{T1}_{pulsed}. For G^{Tn}_{pulsed}, we need to average T1 only over the light period from zero to T_P, and weight it with the excited fraction $k^T_X /(k^T_X+k^T_D)$, as in the cw case.
Then we have:

$$G^{T1}_{pulsed} = S1_{AV} / T1_{AV} \quad \text{and} \quad G^{Tn}_{pulsed} = S1_{AV} / Tn_{AV} \qquad \text{eq. (15)}$$

with

$$S1_{AV} = S_{AV} \cdot k^S_X /(k^S_X+k_{Fl}) \quad \text{and} \quad Tn_{AV} = (1 - S_{AV}) \cdot k^T_X /(k^T_X+k^T_D) \qquad \text{eq. (16)}$$

where

$$S_{AV} = 1/T_R \int_0^{T_P} S(t)\, dt = (k_{RISC}+k_{DARK}) / k_\Sigma \cdot T_P/T_R + k_{FISC} / k_\Sigma \cdot \gamma / k_\Sigma T_P \qquad \text{eq. (17)}$$

and

$$T1_{AV} = 1/T_R \int_0^{T_R} [1- S(t)]\, dt = k_{FISC} / k_\Sigma \cdot [T_P/T_R - \gamma(1/ k_\Sigma T_R + 1/ k_{DARK}\, T_R)] + \Delta T / T_R \qquad \text{eq. (18)}$$

where we introduced $\gamma = [1-\exp(-k_\Sigma T_P)][1-\exp(-k_{DARK}\,\Delta T)]/[1-\exp(-k_\Sigma T_P - k_{DARK}\,\Delta T)]$.

with $\Delta T = T_R - T_P$ being the duration of the dark period between consecutive light pulses (for the detailed derivation of eqs. (17) and (18), see the appendix). In Eq.(17), the first term describes the "losses" (i.e. the steady state average value shortened by T_P/T_R) and the second term describes the "gains", i.e. additional fluorescence from the not yet depleted singlet state. For low excitation energies (i.e. small k_Σ), these gains can be non-negligible, as illustrated in Figure 6A. There exists an optimum for light and dark periods of approximately equal lengths of about 0.7 ms. However, if we consider the *total* fluorescence (Figure 6B), the overall picture is dominated by the "loss" term whose contribution grows linearly with longer pulses and shrinks with longer recovery periods. Therefore, even under optimal pulse timing, the total fluorescence will never exceed the steady state level under continuous illumination.

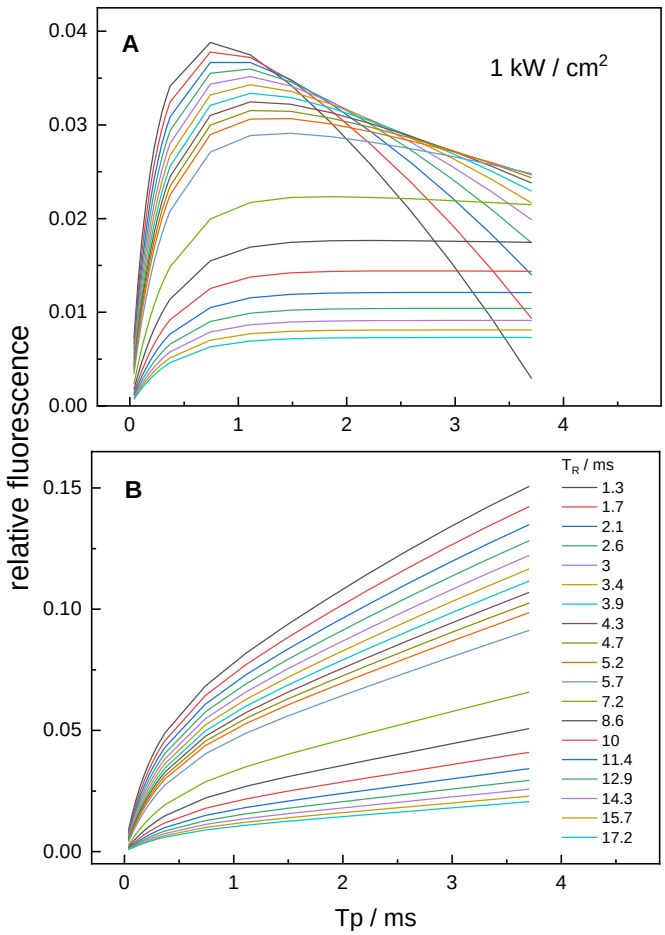

Figure 6 shows the dependence of obtainable fluorescence gain as function of pulse length T_P (x axes) and repetition time T_R (color coded). As expected, the total gain is highest for low excitation rates and becomes rapidly smaller for longer light pulses and dark periods. A, gain term alone (second term in eq (17)), B total fluorescence (both terms in eq. (17)). Note the differing Y-scales.

Even so, concomitantly with the increased averaged singlet population, less average triplet population accumulates; leading in turn to less photobleaching, and consequently the goodness will be improved for pulsed illumination with respect to continuous illumination. In eq (18), the first two terms represent the complement to unity during the light phase (time zero to T_P) and the second two terms describe the triplet population remaining during dark

recovery of the singlet state population (T_P to T_R). To estimate the obtainable gain with respect to the cw situation, we need to replace the total cw population factors for S and T = 1 – S in the cw treatment above (Fig. 3A) with those obtained via equations (17) and (18), while the excited state fractions (Fig. 3B) stay unmodified because establishment of these equilibria S0 ⇔ S1 and T ⇔ Tn is fast (Gigahertz) with respect to millisecond pulsing schemes. To calculate the power density dependent populations under pulsed excitation, we fix T_P and T_R to the optimal values from Fig. 6A as follows:

$$T_R = 0.3 / k_{DARK} = 1.3 \text{ ms} \quad \text{and} \quad T_P = 1 / k_\Sigma \qquad \text{eq. (19)}$$

Thus, T_P will be power dependent via k_X entering both k_{RISC} and k_{FISC} in k_Σ. Moreover, explicit power density dependencies will occur via k_{RISC} and k_{FISC} and in the exponential expression γ, as shown in Figure 7.

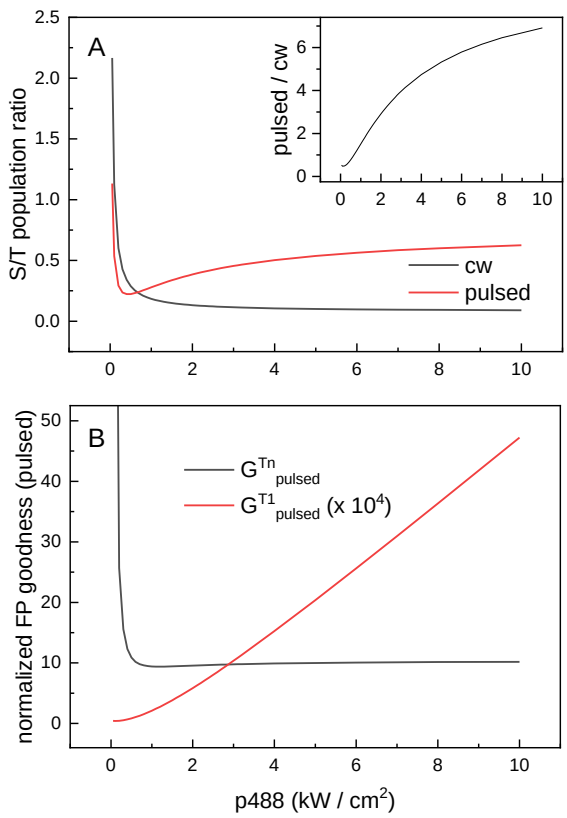

Figure 7. Dependence of singlet-to-triplet manifold populations (eqs.17,18) on excitation power density for continuous (black) and pulsed (red) illumination. Inset, ratio of the two curves in the main panel. A, total populations, B, populations weighted with excited state fractions (equations 15 and 16).

The fact to switch off the excitation light before the singlet population reaches its lowest equilibrium level, allows maintaining the triplet population at a relatively low level, and for higher excitation even more so. This has for consequence that, in contrast to cw excitation, the goodness parameter for conditions of optimal pulse length (red curve in Fig. 7A) does not decrease but increases slightly with excitation power density. Because the cw equilibrium S/T ratio (black curve in Fig. 7A) decreases with increasing power density, for higher excitation, the pulsed-over-continuous gain is higher (Fig. 7A inset) but levels off at a factor of six for the power densities considered here. Interestingly, this gain in effect using pulsed vs CW illumination is of the same order of magnitude as observed for *off*-to-*on* photoswitching rsEGFP2 at CT. [13]

5. Goodness of rsEGFP2 *on* and *off* states at room and cryo temperatures

For the sake of illustration, in this section we will apply the formulae derived in sections 3 and 4 to a popular reversibly switchable FP, viz. rsEGFP2 at RT and CT for its *on* and also for its *off* state. Indeed, for this protein it was found recently, that its *on* state forms a triplet state the absorption spectrum of which is indistinguishable from that of EGFP. In the same work, we published a straightforward means for the detection of triplet state lifetimes via the kinetics of phosphorescence decay.[7] Using the approach and apparatus described there, we also investigated a sample of rsEGFP2 that had been exposed at 100 K to 488 nm illumination until it contained predominantly protein in the *off*-state (Figure 8A, red line). Interestingly, after a short pulse of subsequent 405 nm illumination (exciting exclusively the *off*-state), this sample showed also a phosphorescence decay with a lifetime of 24 ms, just as for the protein in the *on* state. Excitation with 488 nm light as a control showed that this signal did not stem from residual *on* state (Fig. 8B). We thus conclude that the *off* state of rsEGFP2 also forms a triplet state with a 100 K lifetime of 24 ms. Due to limitations in signal-to-noise ratio, we were not able to obtain an absorption spectrum for this state and use therefore that of the *on*-triplet as basis for *off*-state calculations in analogy to those performed in the previous sections for the *on* state, just using the absorption coefficients at 405 nm instead of those at 488 nm.

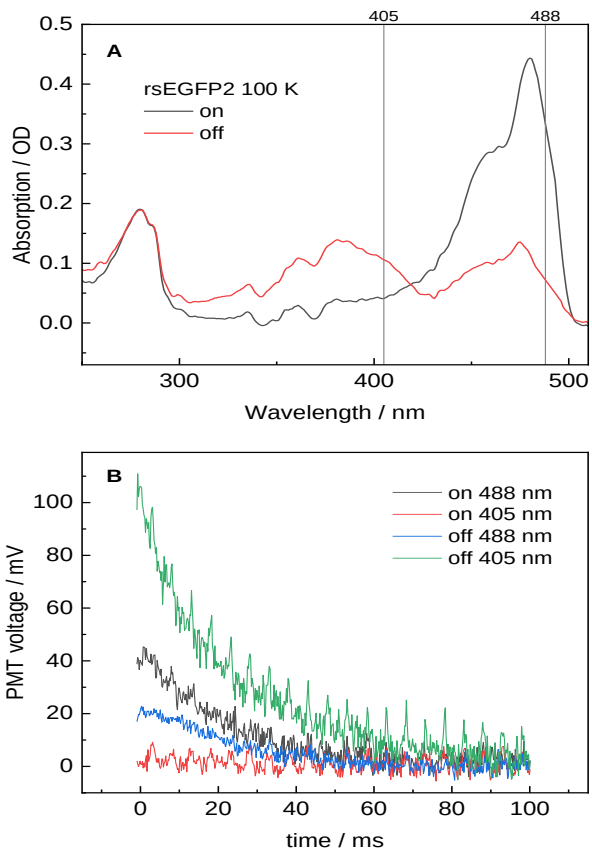

Figure 8. The off-switching of rsEGFP2 reduces 488 nm excited phosphorescence and substantially induces 405 nm excited phosphorescence.
A) absorption spectra of a rsEGFP2 drop before (black) and after (red) 488 nm illumination.
B) decay of rsEGFP2 phosphorescence of the two samples in A) after 20 ms of laser illumination with 1 kW cm^{-2} at 488 nm (black and blue) or 405 nm (red and green) light. All curves decay with a time constant of 24 ms suggesting a common precursor state.

Upon these grounds, we can investigate the respective influence of k_{DARK} and of the singlet and triplet state absorption cross sections (405 vs 488 nm) on k_{RISC} and k_{FISC}. The resulting goodness parameters for both states and both temperatures are summarized in Table 1 for both continuous and pulsed illumination. The values in Table 1 are calculated for 1 kW /cm^2. This excitation power density enters the expressions for k^S_X, k^T_X, k_{FISC}, k_{RISC}, and, via k_Σ also T_P. Consequently, the calculated goodnesses depend in a complicated manner on p and cannot be easily extrapolated from the values in Table 1to other power densities. Therefore, column 2 of

Table 1 indicates the formulae to be used for calculation of various *G* values for other power densities. For the *on* state at RT, *G* values for *p488* up to 10 kW /cm^2 can be read directly from Figs. 5 and 7 for cw and pulsed excitation, respectively. Note also that for the sake of comparability, for pulsed illumination, 1 kW/cm^2 applies only to the light period (and is not corrected to obtain an average of 1 kW/cm^2 over the complete cycle, which would result in higher excitation rates during the light period).

Table 1. Photophysical parameters and resulting photon budgets for rsEGFP2 in the on *and* off *states at RT and CT under illumination of 1 kW /cm^2. Excited state relaxation rate constants k^S_D and k^T_D were set to 10^9 and 10^{10} Hz respectively. G^S was normalized to unity because the value of the intrinsic photobleaching quantum yield is not known precisely. Popular estimates range from 10^{-4} to 10^{-6}. All other goodness values were calculated with G^S=1.This normalization is convenient for straightforward comparison between the different conditions. The actual photon budget, however, is also determined by the fluorescence quantum yield k_{Fl},that naturally is quite different between* on *and* off *states.*

rsEGFP2 1 kW/cm^2	From	*On* RT	*On* CT	*Off* RT	*Off* CT
Wavelength [nm]		488	488	405	405
ε_S [mM $^{-1}$ cm^{-1}]	This work (Fig. 8), Refs. [7], [14]	50	40	25	10
Φ_F	Ref. [7]	0.003	0.003	0.003	0.003
ε_T [mM $^{-1}$ cm^{-1}]	Ref. [7]	10	10	1	1
Φ_R	Ref. [7]	0.001	0.001	0.001	0.001
k_{DARK} [kHz]	$1/\tau_{PH}$	0.233	0.042	0.233	0.042
k^S_X [kHz]	Eq. 6	761	609	315	126
k^T_X [kHz]	Eq. 6	152	152	12.6	12.6
k_{FISC} [kHz]	Eq. 4	2.28	1.83	0.946	0.378
k_{RISC} [kHz]	Eq. 4	0.152	0.152	0.013	0.013
k_Σ [kHz]	Eq. 4	2.67	2.02	1.20	0.433
$T_{steady\ state}$	Eq. 2	0.854	0.904	0.791	0.875
$S_{steady\ state}$	Eq. 2	0.146	0.096	0.209	0.125
S1/S (x 10^3)	Eq. 5	0.76	0.61	0.32	0.13
Tn/T (x 10^3)	Eq. 5	0.015	0.015	0.0013	0.0013
G^S	Eq. 9	1	1	1	1
G^{T1} (x 10^3)	Eq. 12	3.81	1.90	2.5	0.54
G^{Tn}	Eq. 14	8.54	4.24	66.2	14.3
T_P [ms]	Eq. 19	0.37	0.49	0.83	2.3
T_R [ms]	Eq. 19	1.3	7.2	1.3	7.2
S_{AV}	Eq. 17	0.190	0.199	0.211	0.186
T_{AV}	Eq. 18	0.426	0.337	0.574	0.428
G^{T1}_{pulsed} (x 10^3)	Eqs. 15-16	0.338	0.361	0.116	0.0548
G^{Tn}_{pulsed}	Eqs. 15-16	11.7	9.97	66.8	22.8

The numeric values in Table 1 are calculated from the formulae in column two using the photophysical parameters in the first six rows. They are therefore exact values without error bars. However, the uncertainty of the absorption cross sections can be estimated to be in the order of 10%, which relative error will propagate throughout the calculations and as a consequence, the G values listed are also to be taken with such a precision of ±10%.

Comparison of columns 3 with 4 and 5 with 6 shows that, against expectations and observations,[15] lowering the temperature does not increase but rather decrease the photon budget, and this independently on the choice of the precursor state (T1 or Tn) or the illumination scheme (cw or pulsed), with the remarkable exception of G^{T1}_{pulsed} for the *on* state. This effect is due to the fact that at CT, the triplet state lifetime is considerably prolonged and it may speak against the assignment of the triplet state as the (only) photobleaching precursor state. Such a conclusion could also be drawn from comparing G^{T1} between cw and pulsed excitation schemes that always lead to a reduction in photon budget due to the fact that bleaching continues during the dark period if T1 is the precursor state. In contrast, bleaching from Tn occurs only during the (reduced) light period during pulsing and consequently, G^{Tn} is always considerably increased for pulsed illumination (20% at RT and even 100% at CT). The comparison of the G^{T1} and G^{Tn} lines invariably shows orders of magnitude better goodness for the latter but this is somewhat artificial due to the extremely short Tn lifetime and hence vanishing population fraction (see line Tn/T). As G^{T1} increases linearly with excitation power density (both for cw, Fig. 5 and pulsed, Fig. 7), applying MW / cm^2 instead of kW / cm^2 compensates for this effect and renders the absolute G values comparable. Finally, the fact that between *on* and *off* state excitation (488 nm vs 405 nm) both singlet and triplet state absorption differ, but the latter more so, allows for a comparison of the relative impact of these two influences on the photon budget. Naturally, the effect of triplet state absorption is highest on G^{Tn} , where re-excitation of T1 is required. Here, a reduced ε_T results in largely increased photostability. In view of its practical importance, such an effect definitely deserves experimental verification. In contrast to G^{Tn}, G^{T1} appears to scale linearly with ε_S but to vary little with ε_T. If T1 were to be the dominating photobleaching precursor, this would mean that GFP-type FP photon budgets could be improved by choosing excitation wavelength near the singlet state absorption maximum, which again is matter for experimental verification.

6. Discussion

It has long been known that triplet state population plays a decisive role for photobleaching. [16,17] Here we made use of the recently published photophysical parameters for this state for GFP type FPs to propose strategies to optimize a FPs goodness (or photon budget).[7] These should concentrate on the choice of a suitable wavelength of triplet absorption rather than for singlet absorption that, due to its short lifetime, is expected to contribute less to photobleaching.

We saw that in general, increased triplet state lifetime increases the triplet state population and hence photobleaching (e.g. lower photon budget at CT). As a consequence, anaerobic conditions as often strived for in order to minimize ROS creation, may be considered counterproductive, because molecular oxygen acts as an efficient triplet state quencher, reducing EGFP triplet state lifetime more than twice at RT. [6]

Finally, a word is warranted concerning the conditions under which photobleaching is determined experimentally. As discussed, both the excitation power density and the dark decay rate enter the G^T/ G^S correction factors. Therefore, both the illumination conditions (power density at sample position) and the sample environment (e.g. temperature, presence of quenchers in the buffer, e.g. oxygen, see above) will affect the observed photobleaching rates and hence the bleaching yield obtained from them. Moreover, even the experimental setup itself affects the outcome. A broadband light source can excite singlet and triplet state molecules differently than a monochromatic source, a laser scanning excitation acts as a pulsed source whereas wide-field illumination is continuous and even apparently continuous lasers may by construction actually be high frequency pulsed. The formulae introduced here allow on one hand for the due consideration of such influences, and on the other hand for

careful planning of experiments: judicious choice of excitation wavelength, or even use of a second light source for the increase of RISC efficiency, or generally dark state engineering.[18,19] Concerning presence and concentration of potential quenchers of the triplet state, it should be kept in mind that they may also effect the obtainable fluorescence level via direct interaction with the singlet state.[20] Finally, considering the triplet state as potential photobleaching precursor results in non-linear dependence of photobleaching on excitation power density (Figures 5 and 7) and therefore, generally, care is needed in application of a linear photobleaching model for the extraction of numerical photobleaching yields.

7. Conclusion

We have shown the enormous importance of triplet state population dynamics for the photophysical behavior of GFP type proteins at RT and CT, both for continuous and pulsed illumination. We found that consideration of the triplet population yields the photon budget of FPs sometimes almost independent of singlet state absorption but linearly dependent on both excitation power density and RISC brightness, with the y-offset being determined by the dark decay rate. The orders of magnitude higher apparent bleaching yield of FPs as compared to organic dyes such as rhodamines is explained by the long triplet lifetime of the former, having for consequence a higher steady state triplet population. Use of sub-millisecond excitation pulses with kHz repetition rates is proposed to remedy these effects to a certain extent. Formulae are derived that allow to simulate the fluorescence and photobleaching outcome for various conditions as function of molecular parameters such as fluorescence lifetime, triplet formation and decay yields and lifetimes, as well as pulse timing (duration, frequency). Further experimental investigation of the proposed photobleaching pathways is crucially necessary but even before that will be accomplished, the possibility of photobleaching via the triplet state should be seriously taken into account for the planning of biological fluorescence microscopy experiments, especially at power densities as routinely used for single molecule detection.

Acknowledgements

We thank Ninon Zala (Grenoble) for the skillful preparation of the protein samples. The IBS acknowledges integration into the Interdisciplinary Research Institute of Grenoble (IRIG, CEA).

Conflict of interest

The authors declare no conflict of interest.

Appendix

Derivation of eqs. (17, 18) for averaged populations under pulsed illumination. Following the approach by Gregor et al., [12] we consider the simplest possible two state model (Scheme 1A). Under illumination, we have:
$k1 = k_{FISC}$ and $k2 = k_{RISC} + k_{DARK}$, while in obscurity we will have $k1 = 0$ and $k2 = k_{DARK}$. For normalized total population S + T = 1, under these conditions the total singlet population S will evolve as follows for light (eq. 20) and dark (eq. 21) conditions:

$$S^{light}(t) = (k_{RISC} + k_{DARK}) / k_{\Sigma} \cdot [1+ \alpha \exp(-k_{\Sigma}\, t)] \qquad \text{eq. (20)}$$

$$S^{dark}(t) = 1 - \beta \exp[- k_{DARK}(t-T_P)] \qquad \text{eq.(21),}$$

where α and β are amplitude constants that can be determined from equating the populations of eqs (20) and (21) at time points $t = T_P$ (eq. 22) and $t = 0 = T_R$ (eq. 23) (see Scheme 2):

$$(k_{RISC} + k_{DARK})/ k_{\Sigma} \cdot [1 + \alpha \exp(-k_{\Sigma} T_P)\} = 1 - \beta \qquad \text{eq. (22)}$$

$$(k_{RISC} + k_{DARK})/ k_{\Sigma} \cdot (1 + \alpha) = 1 - \beta \exp[- k_{DARK}(T_R-T_P)] \qquad \text{eq.(23).}$$

Upon rearrangement, we obtain:

$$\alpha = k_{FISC} / (k_{RISC} + k_{DARK}) \cdot [1-\exp(-k_{DARK}\Delta T)] / [1-\exp(-k_{\Sigma} T_P - k_{DARK}\Delta T)] \qquad \text{eq. (24)}$$

$$\beta = k_{FISC} / k_{\Sigma} \cdot [1-\exp(-k_{\Sigma} T_P)] / [1-\exp(-k_{\Sigma} T_P - k_{DARK}\Delta T)] \qquad \text{eq. (25).}$$

with $\Delta T = T_R - T_P$ and $k_{\Sigma} = k_{FISC} + k_{RISC} + k_{DARK}$. The time average of the singlet population contributing to fluorescence during one complete light/dark cycle is then given by eq. (26), where the integration over the S population is done exclusively over the light period from t=0 to t = T_P. This is because no excitation light is present during the dark recovery period, hence no fluorescence is excited even if potentially fluorescent singlet molecules are available.

$$S_{AV} = 1/T_R \int_0^{T_P} S^{light}(t)\, dt \qquad \text{eq. (26)}$$

Substituting equations (20) and (24) into eq. (26) and performing the integration yields eq. (17) for the average fluorescing singlet population.

$$S_{AV} = (k_{RISC} + k_{DARK})/ k_{\Sigma} \cdot T_P / T_R$$
$$+ k_{FISC} / k_{\Sigma} \cdot 1/ k_{\Sigma} T_R \cdot [1-\exp(-k_{DARK}\Delta T)]\, [1-\exp(-k_{\Sigma} T_P)] / [1-\exp(-k_{\Sigma} T_P - k_{DARK}\Delta T)]$$

The complement to unity will give the fraction of the triplet population that is prone to photobleaching during the light period. In view of the fact that in case of a T1 precursor state for photobleaching, no further excitation is needed, the average triplet population needs to be calculated including the singlet recovery during the dark period T_P toT_R, yielding eq. (27):

$$T1_{AV} = 1/T_R \int_0^{T_R} [1- S(t)]\, dt = 1/T_R \left(\int_0^{T_P} [1- S^{light}(t)]\, dt + \int_{T_P}^{T_R} [1-S^{dark}(t)]\, dt\right) \qquad \text{eq. (27)}$$

Substituting equations (20),(21), (24) and (25) into eq. (27) and performing the integration yields eq. (18) for the triplet population averaged over one complete light/dark cycle.

References

[1] T. Hirschfeld, *Appl. Opt.* **1976**, *15*, 3135–3139.
[2] I. Urbančič, Z. Arsov, A. Ljubetič, D. Biglino, J. Štrancar, *Optics Express* **2013**, *21*, 25291.
[3] D. Wüstner, T. Christensen, L. Solanko, D. Sage, *Molecules* **2014**, *19*, 11096–11130.
[4] T. J. Lambert, *Nature Methods* **2019**, *16*, 277–278.
[5] P. J. Cranfill, B. R. Sell, M. A. Baird, J. R. Allen, Z. Lavagnino, H. M. de Gruiter, G.-J. Kremers, M. W. Davidson, A. Ustione, D. W. Piston, *Nat Meth* **2016**, *13*, 557–562.
[6] M. Byrdin, C. Duan, D. Bourgeois, K. Brettel, *Journal of the American Chemical Society* **2018**, *140*, 2897–2905.
[7] L. Rane, J. Wulffele, D. Bourgeois, O. Glushonkov, A. M. R. Mantovanelli, N. Zala, M. Byrdin, *J. Phys. Chem. B* **2023**, *127*, 5046–5054.
[8] F. Bierbuesse, A. C. Bourges, V. Gielen, V. Mönkemöller, W. Vandenberg, Y. Shen, J. Hofkens, P. Vanden Berghe, R. E. Campbell, B. Moeyaert, P. Dedecker, *Nat Commun* **2022**, *13*, 1850.
[9] A. C. Bourges, B. Moeyaert, T. Y. H. Bui, F. Bierbuesse, W. Vandenberg, P. Dedecker, *Chem. Commun.* **2023**, DOI 10.1039/D3CC01617J.
[10] G. Donnert, C. Eggeling, S. W. Hell, *Nat Meth* **2007**, *4*, 81–86.
[11] C. Ringemann, A. Schonle, A. Giske, C. von Middendorff, S. W. Hell, C. Eggeling, *Chemphyschem* **2008**, *9*, 612–624.
[12] I. Gregor, D. Patra, J. Enderlein, *ChemPhysChem* **2005**, *6*, 164–170.
[13] A. M. R. Mantovanelli, O. Glushonkov, V. Adam, J. Wulffelé, D. Thédié, M. Byrdin, I. Gregor, O. Nevskyi, J. Enderlein, D. Bourgeois, *J. Am. Chem. Soc.* **2023**, jacs.3c01500.
[14] V. Adam, K. Hadjidemetriou, N. Jensen, R. L. Shoeman, J. Woodhouse, A. Aquila, A. Banneville, T. R. M. Barends, V. Bezchastnov, S. Boutet, M. Byrdin, M. Cammarata, S. Carbajo, N. Eleni Christou, N. Coquelle, E. De la Mora, M. El Khatib, T. Moreno Chicano, R. Bruce Doak, F. Fieschi, L. Foucar, O. Glushonkov, A. Gorel, M. L. Grünbein, M. Hilpert, M. Hunter, M. Kloos, J. E. Koglin, T. J. Lane, M. Liang, A. Mantovanelli, K. Nass, G. Nass Kovacs, S. Owada, C. M. Roome, G. Schirò, M. Seaberg, M. Stricker, M. Thépaut, K. Tono, K. Ueda, L. M. Uriarte, D. You, N. Zala, T. Domratcheva, S. Jakobs, M. Sliwa, I. Schlichting, J. Colletier, D. Bourgeois, M. Weik, *ChemPhysChem* **2022**, DOI 10.1002/cphc.202200192.
[15] C. L. Schwartz, V. I. Sarbash, F. I. Ataullakhanov, J. R. McIntosh, D. Nicastro, *Journal of Microscopy* **2007**, *227*, 98–109.
[16] L. A. Deschenes, D. A. Vanden Bout, *Chemical Physics Letters* **2002**, *365*, 387–395.
[17] V. Jacques, J. D. Murray, F. Marquier, D. Chauvat, F. Grosshans, F. Treussart, J. F. Roch, *Applied Physics Letters* **2008**, *93*, DOI 10.1063/1.3013843.
[18] B. Peng, R. Dikdan, S. E. Hill, A. C. Patterson-Orazem, R. L. Lieberman, C. J. Fahrni, R. M. Dickson, *J. Phys. Chem. B* **2021**, *125*, 5200–5209.
[19] L. Ludvikova, E. Simon, M. Deygas, T. Panier, M.-A. Plamont, J. Ollion, A. Tebo, M. Piel, L. Jullien, L. Robert, T. Le Saux, A. Espagne, *Nat Biotechnol* **2023**, DOI 10.1038/s41587-023-01893-7.
[20] J. M. Murray, *Journal of Microscopy* **2017**, *267*, 193–213.